AUGUST 01 1983

Sound radiation from an impact-excited clamped circular plate in an infinite baffle

Adnan Akay; Michael Latcha

J. Acoust. Soc. Am. 74, 640–648 (1983)
https://doi.org/10.1121/1.389787

Sound radiation from an impact-excited clamped circular plate in an infinite baffle

Adnan Akay and Michael Latcha
Mechanical Engineering Department, Wayne State University, Detroit, Michigan 48202

(Received 7 September 1982; accepted for publication 13 February 1983)

Sound radiation from most mechanical systems results from impact forces of various kinds. In this paper, transient sound radiation from impact-excited circular plates is studied both analytically and experimentally. First, the contact force developed during the inelastic collision of a ball with a flexible plate was obtained. The plate vibrations were then obtained using normal mode analysis. The sound radiation waveforms in the time domain were obtained by numerical integration of the Rayleigh integral. Both analytical and experimental results show the radiation of a sound pulse during the contact which is a result of the forced deformation of the plate. Quantitative relationships are given for the plate vibration response and acoustic radiation.

PACS numbers: 43.20.Px, 43.40.Dx, 43.20.Tb

INTRODUCTION

Sound radiation from elastic structures excited by impact forces is a fundamental problem in acoustics. Most mechanical systems exhibit impact forces of various kinds. The mechanism of sound radiation resulting from mechanical impacts may differ according to the geometry and the nature of contact between the impinging objects.[1] In general, the dynamic response of an impacted object can be considered as its forced and free vibrations. The forced response of an object may be its acceleration as a whole, resulting in rigid-body radiation, or it may be rapid deformation of its surfaces, which results in a different radiation mechanism. On the other hand, the free vibrations of an object following impact result in what is commonly called "ringing" radiation.

The first investigation of sound radiation from impacted plates was done by Strasberg,[2] who calculated the radiated acoustic power from a periodically struck diaphragm in the frequency domain. The formulation of the radiation problem was based on earlier results of Lax,[3] who investigated radiation loading on a circular clamped plate using the Rayleigh integral equation. Several other studies on sound radiation from impacted plates have led to empirical relationships between sound pressure amplitude and plate vibration response in different frequency regions. These experimental studies have also established relationships between the radiated peak sound pressure amplitudes and the momentum or kinetic energy of the impacting spheres on elastic plates.[4–8] In addition, a number of analytical studies have been reported on radiation from infinite plates excited by point forces[9–11] and transient sound transmission through finite plates.[12–16] These studies, however, have not addressed the problem of transient sound radiation from finite plates. In a recent paper on paper noise in impact line printers, expressions for the sound power radiation from the forced and free vibrations of a sheet of paper were modeled as a simply supported rectangular plate, with results given in the frequency domain.[17]

In this paper, transient sound radiation from the forced and free vibrations of a circular elastic plate in an infinite baffle excited by an impact force is examined. Solutions of the pressure waveform are obtained by numerical integration of the Rayleigh integral. These results are compared with corresponding measured waveforms.

I. VIBRATION RESPONSE OF THE PLATE

The vibration response of a clamped circular plate to an impact force can be found by solving the classical equation of motion of the plate in Eq. (1)

$$D(1+j\eta)\nabla^4 u(r,\theta,t) + \rho h \frac{\partial^2 u(r,\theta,t)}{\partial t^2} = F(r,\theta,t), \qquad (1)$$

where $u(r,\theta,t)$ is the displacement of the plate at a point (r,θ) and $F(r,\theta,t)$ is the applied force per unit area of the plate. The constants in Eq. (1) are $D = Eh^3/12(1-\nu^2)$ is the flexural rigidity, ρ is the density, h is the thickness, E is Young's modulus, ν is Poisson's ratio, and η is the internal loss factor of the plate. Although the Euler plate theory is used here to describe the vibration response of the plate, Timoshenko–Mindlin plate theory should be used to avoid the slight error introduced in the frequency response for frequencies above which $8\lambda_p < h$, where λ_p is the plate wavelength.[11] It should be noted also that, in general, neglect of fluid loading on the plate shifts frequencies and alters the mode shapes. However, for radiation from plates of common metals into air this change is negligible.[3]

The displacement response of a circular plate, initially undeformed and at rest, to an arbitrary force $F(r,\theta,t)$ can be written as

$$u(r,\theta,t) = \frac{1}{\rho h} \sum_{n=0}^{\infty} \sum_{m=0}^{\infty} \frac{\phi_{nm}(r,\theta)}{\omega_{nm}(1+j\eta)^{1/2}} \int_0^t F_{nm}(\tau) \times \sin\left[\omega_{nm}(1+j\eta)^{1/2}(t-\tau)\right] d\tau, \qquad (2)$$

where ω_{nm} are the natural frequencies of the plate, with the subscripts n,m denoting the radial and circular modes, respectively. ϕ_{nm} are the normal mode shapes of the plate and are determined by applying the boundary conditions to the homogeneous, undamped equation of motion of the plate. For the axisymmetric vibrations of a clamped circular plate of radius a the normalized mode shapes are given by

$$\phi_n(r) = \frac{1}{\sqrt{2}}\left(\frac{J_0(\lambda_n r/a)}{J_0(\lambda_n)} - \frac{I_0(\lambda_n r/a)}{I_0(\lambda_n)}\right), \tag{3}$$

where λ_n are the roots of the frequency equation

$$J_0(\lambda_n)I_1(\lambda_n) + J_1(\lambda_n)I_0(\lambda_n) = 0.$$

J_0 and J_1 are Bessel functions of the first kind and I_0 and I_1 are modified Bessel functions of the first kind. The natural frequencies of the plate ω_n are given by

$$\omega_n = (\lambda_n/a)^2 (D/\rho h)^{1/2}. \tag{4}$$

A. The impact force

The expression for the contact force developed during elastic impact of a spherical striker of radius b with a rigid plane surface of a semi-infinite solid was given by Hunter[18] as a function of the relative approach "α" of the striker and the impacted plane surface:

$$F(t) = k\alpha(t)^{3/2}, \tag{5}$$

where

$$k = \frac{4}{3}\sqrt{b}\left(\frac{(1-\nu_1^2)}{E_1} + \frac{(1-\nu)^2}{E}\right)^{-1},$$

ν_1, ν and E_1, E are Poisson's ratios and elasticity moduli of the sphere and the impacted object, respectively. The contact-force expression given in Eq. (5) is an extension of the well-known Hertz contact theory developed for the static contact of curved bodies.[19,20]

Although Eq. (5) was obtained for plates of semi-infinite thickness, it is applicable to thick plates, or slabs, where the time taken for the elastic waves to reflect from the lower surface of the plate back to the impact region is much longer than the contact duration. As the thickness of the plate, or its impedance, is decreased the contact force between the sphere and the plate deviates sharply from that predicted by Hertz theory.

In the case of impact of a sphere with a thin plate, the force-time history is found by combining Eq. (5) with the equation of motion (1) of the plate.[21–23] The resulting nonlinear differential equation obtained by Zener[22] for the case of a large plate (where the reflections from the boundaries of the plate return to the impact region after the contact ceases) is given as

$$F\frac{d^2F}{dt^2} - \frac{1}{3}\left(\frac{dF}{dt}\right)^2 + \frac{3}{2}k^{3/2} \times\left(\frac{1}{m_1}F^{7/3} + \frac{3(1-\nu^2)}{4h^2\rho E}F^{4/3}\frac{dF}{dt}\right) = 0. \tag{6}$$

Following Zener,[22] Eq. (6) is nondimensionalized to give

$$\frac{d^2\sigma}{d\tau^2} + \left(1 + \lambda\frac{d}{d\tau}\right)\sigma^{3/2} = 0, \tag{7}$$

where $\tau = t/T$, $\sigma = \alpha/TU_0$, and $T = 0.311T_H$. T_H is the duration of the impact predicted by Hertz theory for infinitely rigid surfaces and is given by $T_H = 2.9432\,\alpha_m/U_0$. $\alpha_m = (5U_0^2 m_1/4k)^{2/5}$ is the maximum value of the relative displacement α, and U_0 is the impact velocity.

Equation (7) depends on a nondimensional constant λ called the "inelasticity parameter" and is given by $\lambda = 3.218 \times m_1/T_H Z$, where m_1 is the mass of the striker and $Z = 8(D\rho h)^{1/2}$ is the impedance of the plate at the impact position.

The force-time history obtained from Eq. (7) is plotted for various values of the inelasticity parameter λ in Fig. 1.[22] In cases for which λ is very small, the contact-time history resembles the square of a half-period sine wave.[21] As the value of λ increases, the impact force amplitude decreases and the duration of contact is longer in the second half of the contact period. The maximum value of the normalized impact force decays exponentially with λ as shown in Fig. 2. Since the inelasticity parameter λ is inversely proportional to the second power of plate thickness h, for a given impact velocity the impact force amplitude increases nonlinearly with plate thickness and mass of the striker, reaching its maximum value predicted by Hertz theory for a plate of semi-infinite thickness.

In this paper the force developed during impact between a spherical impactor and a plate is represented as a point force with a squared half-period sine-wave time history.

$$F(r,t) = F_0\delta(r)\sin^2\omega_0 t/2\pi r, \quad 0 \leqslant t \leqslant \pi/\omega_0, \tag{8}$$

where the duration of contact $T_H = \pi/\omega_0$ is obtained from the Hertz theory and the amplitude F_0 is obtained by using the inelasticity parameter following the analysis described above. It should be noted that, although impact force is sometimes defined as a half-period sine pulse, the discontinuities in the rate of change of this force-time history induce artificially high frequencies in the dynamic response of the system. Therefore, the force-time waveform should have a continuous derivative. The effects of a half-period sine pulse and its powers as the force waveform are shown in the fol-

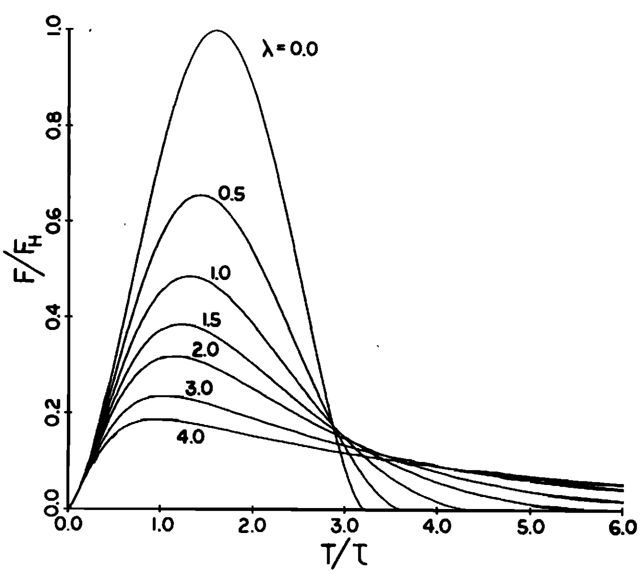

FIG. 1. Normalized impact-force time history for various inelasticity parameters.

lowing section. Also, care must be taken in the assumption of a "point force" for the spatial distribution of the impact force, since it implies that the eigenfunctions are constant in the contact region, which may not be true at very high frequencies.

B. Response of the plate to impact

The axisymmetric displacement response of a circular plate with clamped outer edge to an impact force by a spherical object can be found by evaluating the response in Eq. (2) with the forcing function in Eq. (8), which gives

$$u(r,t) = \frac{F_0}{M} \sum_{n=0}^{\infty} \frac{\phi_n(0)\phi_n(r)}{(4\omega_0^2 - \omega_n^2)\sin\Omega - 2\eta\omega_n\omega_0\cos\Omega} \begin{cases} \frac{1}{2}\sin(2\omega_0 t + \Omega) + X_1 e^{-(\eta/2)\omega_n t}\sin(\omega_n^* t + \Omega_1) + E, & 0 < t \leqslant \pi/\omega_0 \\ X_2 e^{-(\eta/2)\omega_n t_1}\sin(\omega_n^* t_1 + \Omega_2), & t_1 = t - \pi/\omega_0 \geqslant 0, \end{cases} \tag{9}$$

where

$$\Omega = \tan^{-1}[(\omega_n^2 - 4\omega_0^2)/2\eta\omega_0\omega_n],$$

$$\Omega_1 = \tan^{-1}\left(\frac{\omega_n^*(E + \frac{1}{2}\sin\Omega)}{\omega_0\cos\Omega + \frac{1}{2}\eta\omega_n(E + \frac{1}{2}\sin\Omega)}\right),$$

$$\Omega_2 = \tan^{-1}[C_1\omega_n^*/(C_2 + \tfrac{1}{2}C_1\eta\omega_n)],$$

$$X_1 = \omega_0\cos\Omega/(\tfrac{1}{2}\eta\,\omega_n\sin\Omega_1 - \omega_n^*\cos\Omega_1),$$

$$X_2 = C_2/(\omega_n^*\cos\Omega_2 - \tfrac{1}{2}\eta\omega_n\sin\Omega_2),$$

$$C_1 = \tfrac{1}{2}\sin\Omega + X_1\exp(-\eta\omega_n\pi/2\omega_0)\sin(\omega^*\pi/\omega_0 + \Omega_1) + E,$$

$$C_2 = \omega_0\cos\Omega + X_1\exp(-\eta\omega_n\pi/2\omega_0) \times [\omega_n^*\cos(\omega_n^*\pi/\omega_0 + \Omega_1) - (\eta/2)\omega_n\sin(\omega_n^*\pi/\omega_0 + \Omega_1)],$$

$$E = [(4\omega_0^2 - \omega_n^2)\sin\Omega - 2\eta\omega_0\omega_n\cos\Omega]/2\omega_n^2,$$

$$M = \rho\pi a^2 h, \quad \text{and } \omega_n^* = \omega_n(1 - \eta^2/4)^{1/2}.$$

The velocity and acceleration response of the plate are obtained by differentiating Eq. (9) once and twice, respectively. Examples of these waveforms at the center of the plate opposite from the impact point are shown in Fig. 3 for the cases of impact of a 1.905-cm-diam acrylic ball on a 1.59-mm-thick steel plate of 0.50-m diameter. The acceleration response obtained from Eq. (9) is used in the following section to obtain the sound pressure radiated from a circular plate.

II. TRANSIENT RADIATION FROM A CIRCULAR PLATE

The acoustic pressure from a plate vibrating in an infinite baffle is calculated by using the Rayleigh surface integral where each elemental area on the plate surface is regarded as a simple point source of an outgoing wave and their contributions are added with appropriate time delay[24]

$$P(R,\theta,\psi,t) = \frac{\rho_0}{2\pi}\int\!\!\int \ddot{u}\left(r,\theta,t - \frac{d}{c}\right)\frac{dS}{d}, \tag{10}$$

where $\ddot{u}(r,\theta,t)$ is the acceleration-time response of the plate and d is the distance from each elemental area to the field point as shown in Fig. 4. The Rayleigh integral is a special case of the Helmholtz–Huygens integral for a plane radiator in a rigid infinite baffle where reflection or diffraction of sound does not take place at the boundaries.

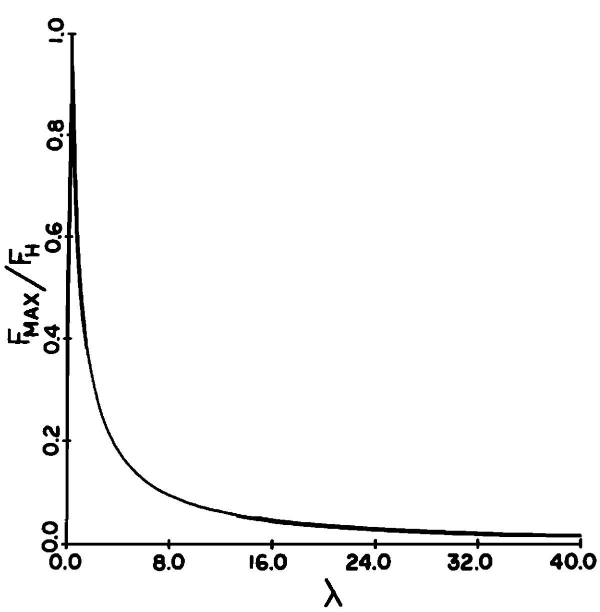

FIG. 2. Impact force amplitude as a function of plate inelasticity.

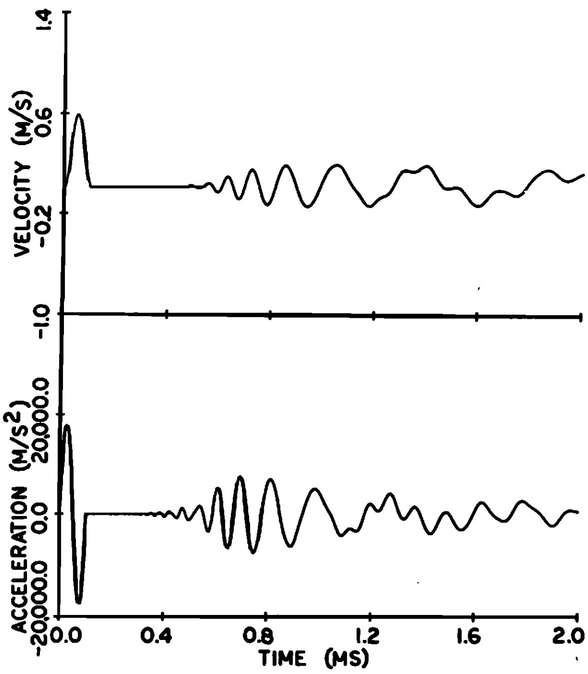

FIG. 3. Velocity and acceleration response of the plate at the impact point. 1.905-cm-acrylic ball and 1.59-mm-thick steel plate. $H = 0.10$ m.

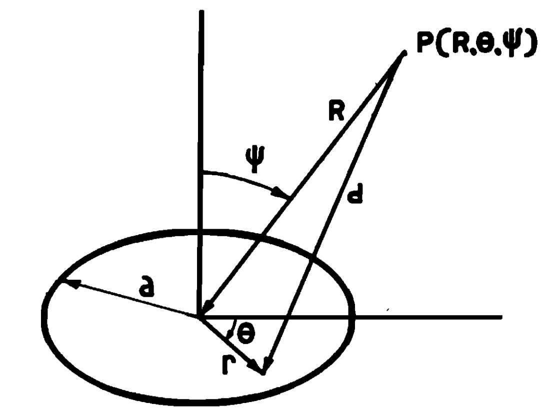

FIG. 4. Geometry of the problem.

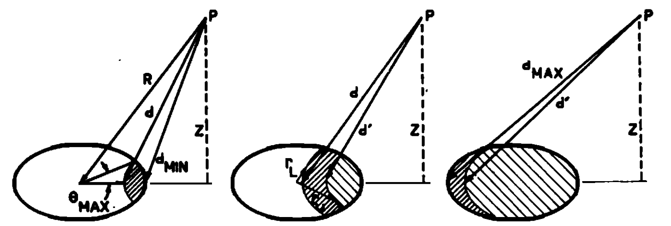

FIG. 5. Integral limits for $R\sin\psi>a$: (i) When $d<R$: $r_L(\theta,d)=R\sin\psi\times\cos\theta-(d^2-R^2\cos^2\psi-R^2\sin^2\psi\sin^2\theta)^{1/2}$, $r_u=a$, and θ changes from $-\theta_{\max}$ to $\theta_{\max}$; (ii) When $d>R$, integration is performed in two steps. When $0<\theta<\theta_{\max}$: $r_L=0$ and $r_u=R\sin\psi-(d^2_{\min}-R^2\cos^2\psi)^{1/2}$. When $\theta_{\max}<\theta$: $r_L=0$, $r_u=R\sin\psi\cos\theta+(d^2-R^2\cos\psi-R^2\sin^2\psi\times\cos^2\theta)^{1/2}$, and θ changes from $\theta_{\max}$ to $(\theta_{\max}+\pi)$, where $\theta_{\max}=\cos^{-1}\times[(z^2-d^2+a^2+R^2\sin\psi)/2aR\sin\psi]$.

A. Boundary conditions

For steady-state radiation problems the surface integral in Eq. (10) is carried out over the area of the plate and the proper time delay due to the distance from the receiver to various parts of the plate is accounted for by the time-delay term $t-d/c$ in the integrand. However, for time-dependent vibrations of a plate such as the beginning or conclusion of vibrations or turning on or off of a source, the integral limits in Eq. (10) are time dependent. These integration limits must account for the early arrival of radiation from the elemental areas closer to the receiver point at the start of the radiation and for the late arrival of the waves from the distant areas of the plate at the conclusion of radiation. The Rayleigh integral is then evaluated piecewise using time-dependent integration limits with appropriate contribution of forced and free acceleration responses of the plate, $\ddot{u}_1$ and $\ddot{u}_2$, respectively. These integral limits are illustrated in Figs. 5 and 6 and are given in Table I for different geometric configurations of the receiver point with respect to the plate, and for different impact force durations compared with the time it takes for the sound waves to reach from the plate to the receiver point.

B. Evaluation of the Rayleigh integral

Substitution of the axisymmetric plate acceleration waveform, obtained by twice differentiating the displacement response in Eq. (9) into the Rayleigh integral in Eq. (10), gives

$$p(R,\psi,t)=\frac{\rho_0F_0}{2\pi M}\sum_{n=0}^{\infty}\frac{\phi_n(0)}{(4\omega_0^2-\omega_n^2)\sin\Omega-2\eta\omega_n\omega_0\cos\Omega}\int_{\theta_L}^{\theta_u}\int_{r_L}^{r_u}A\left(r,\theta,t-\frac{d}{c}\right)\phi_n(r)\frac{r\,dr\,d\theta}{d},\tag{11}$$

where

$$A(r,\theta,t-d/c)=\begin{cases}-2\omega_0^2\sin\left(2\omega_0t-2\omega_0\dfrac{d}{c}+\Omega\right)+X_1\exp\left[-\dfrac{1}{2}\eta\omega_n\left(t-\dfrac{d}{c}\right)\right]\\ \quad\times\left[\left(\dfrac{\eta^2}{4}\omega_n^2-\omega_n^{*2}\right)\sin\left(\omega_n^*t-\omega_n^*\dfrac{d}{c}+\Omega_1\right)-\eta\omega_n\omega_n^*\cos\left(\omega_n^*t-\omega_n^*\dfrac{d}{c}+\Omega_1\right)\right], & 0<t\leqslant\dfrac{\pi}{\omega_0}\\ X_2\exp\left[-\dfrac{1}{2}\eta\omega_n\left(t_1-\dfrac{d}{c}\right)\right]\left[\left(\dfrac{\eta^2}{4}\omega_n^2-\omega_n^{*2}\right)\sin\left(\omega_n^*t_1-\omega_n^*\dfrac{d}{c}+\Omega_2\right)\right.\\ \quad\left.-\eta\omega_n\omega_n^*\cos\left(\omega_n^*t_1-\omega_n^*\dfrac{d}{c}+\Omega_2\right)\right], & t_1>0\end{cases}$$

and

$$t_1=t-\pi/\omega_0,\quad d=(r^2+R^2-2rR\sin\psi\cos\theta)^{1/2}.$$

Equation (11) can be rewritten in the following form using trigonometric identities:

$$p(R,\psi,t)=\frac{\rho_0F_0}{2\pi M}\sum_{n=0}^{\infty}\frac{\phi_n(0)}{(4\omega_0^2-\omega_n^2)\sin\Omega-2\eta\omega_n\omega_0\cos\Omega}\begin{cases}[A_1I_1+A_2I_2+(A_3+A_5)I_3+(A_4+A_6)I_4], & 0<t\leqslant\pi/\omega_0\\ [(B_1+B_3)I_3+(B_2+B_4)I_4], & \pi/\omega_0<t\end{cases},\tag{12}$$

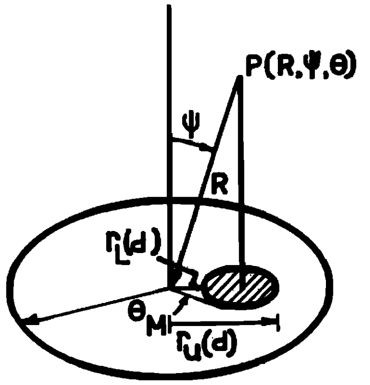

FIG. 6. Integral limits for $R\sin\psi<a$: (i) When $(d^2-R^2\cos^2\psi)^{1/2}<(a-R\sin\psi)$: $r_L=R\sin\psi\cos\theta-(d^2-R^2\cos^2\psi-R^2\sin^2\psi\sin^2\theta)^{1/2}$, $r_u=R\sin\psi\cos\theta+(d^2-R^2\cos^2\psi-R^2\sin^2\psi\sin^2\theta)^{1/2}$, and $\theta_L=-\theta_{\max}$, $\theta_u=+\theta_{\max}$; (ii) When $(d^2-R^2\cos^2\psi)>(a-R\sin\psi)$ integration is performed in two steps: When $0<\theta<\theta_{\max}$: $r_L=0$ and $r_u=R\sin\psi-(d^2_{\min}-R^2\cos^2\psi)^{1/2}$. When $\theta_{\max}<0$: $r_L=0$, $r_u=R\sin\psi\cos\theta+(d^2-R^2\cos\psi-R^2\sin^2\psi\cos^2\theta)^{1/2}$, and θ changes from $\theta_{\max}$ to $(\theta_{\max}+\pi)$, where $\theta_{\max}=\sin^{-1}[(d^2-R^2\cos^2\psi)^{1/2}/R\sin\psi]$.

where

$$
\begin{aligned}
A_1 &= -2\omega_0^2\sin(2\omega_0 t+\Omega),\\
A_2 &= 2\omega_0^2\cos(2\omega_0 t+\Omega),\\
A_3 &= X_1(\tfrac{1}{4}\eta^2\omega_n^2-\omega_n^{*2})e^{-1/2\eta\omega_n t}\sin(\omega_n^* t+\Omega_1),\\
A_4 &= -X_1(\tfrac{1}{4}\eta^2\omega_n^2-\omega_n^{*2})e^{-1/2\eta\omega_n t}\cos(\omega_n^* t+\Omega_1),\\
A_5 &= -X_1\eta\omega_n\omega_n^* e^{-1/2\eta\omega_n t}\cos(\omega_n^* t+\Omega_1),\\
A_6 &= -X_1\eta\omega_n\omega_n^* e^{-1/2\eta\omega_n t}\sin(\omega_n^* t+\Omega_1),\\
B_1 &= +X_2 e^{-1/2\eta\omega_n t_1}[(\eta^2/4)\omega_n^2-\omega_n^{*2}]\sin(\omega_n^* t_1+\Omega_2),\\
B_2 &= -X_2 e^{-1/2\eta\omega_n t_1}[(\eta^2/4)\omega_n^2-\omega_n^{*2}]\cos(\omega_n^* t_1+\Omega_2),\\
B_3 &= -X_2 e^{-1/2\eta\omega_n t_1}\eta\omega_n\omega_n^*\cos(\omega_n^* t_1+\Omega_2),\\
B_4 &= -X_2 e^{-1/2\eta\omega_n t_1}\eta\omega_n\omega_n^*\sin(\omega_n^* t_1+\Omega_2),
\end{aligned}
\tag{13}
$$

and the integrals I are given as

$$I_1=\int\int_S\cos\left(\frac{2\omega_0 d}{c}\right)\frac{\phi_n(r)r\,dr\,d\theta}{d},\tag{14a}$$

$$I_2=\int\int_S\sin\left(\frac{2\omega_0 d}{c}\right)\frac{\phi_n(r)r\,dr\,d\theta}{d},\tag{14b}$$

$$I_3=\int\int_S\exp\left(\frac{\eta\omega_n d}{2c}\right)\cos\left(\frac{\omega_n^* d}{c}\right)\frac{\phi_n(r)r\,dr\,d\theta}{d},\tag{14c}$$

$$I_4=\int\int_S\exp\left(\frac{\eta\omega_n d}{2c}\right)\sin\left(\frac{\omega_n^* d}{c}\right)\frac{\phi_n(r)r\,dr\,d\theta}{d}.\tag{14d}$$

The integrals in Eqs. (14) are solved here for the case of a receiver point on the axis-of-symmetry of the plate using the time-dependent boundary conditions given in Table I.

Sound radiation from elemental areas on the plate with equal radial distances from the plate center arrive simultaneously at receiver points located on the axis-of-symmetry of the plate. The time-dependent integration limits represent

TABLE I. Integration limits for Eq. (12) for various conditions.

I. $R\sin\psi>a$	
(a) $\pi/w_0<d_{\max}/c$	
(i) $d_{\min}<ct<d_{\min}+\pi c/w_0$	$\ddot{u}_1$: $r_L(d)\mapsto a$,
(ii) $d_{\min}+\pi c/w_0<ct<d_{\max}$	$\ddot{u}_1$: $r_L(d)\mapsto r_u(d')$
	$\ddot{u}_2$: $r_u(d')\mapsto a$
(iii) $d_{\max}<ct<d_{\max}+\pi c/w_0$	$\ddot{u}_1$: $0\to a$
	$-\ddot{u}_1$: $r_L(d')\mapsto a$
	$\ddot{u}_2$: $r_L(d')\mapsto a$
(iv) $d_{\max}+\pi c/w_0<ct$	$\ddot{u}_2$: $0\to a$
(b) $\pi/w_0>d_{\max}/c$	
(i) $d_{\min}<ct<d_{\max}$	$\ddot{u}_1$: $r_L(d)\mapsto a$
(ii) $d_{\max}<ct<d_{\max}+\pi c/w_0$	$\ddot{u}_1$: $0\to a$
(iii) $d_{\max}+\pi c/w_0<ct<2d_{\max}+\pi c/w_0$	$\ddot{u}_1$: $0\to a$
	$-\ddot{u}_1$: $r_L(d')\mapsto a$
	$\ddot{u}_2$: $r_L(d')\mapsto a$
(iv) $2d_{\max}+\pi c/w_0<ct$	$\ddot{u}_2$: $0\to a$
where $d=d_{\min}+ct$	
$d'=d_{\min}+c(t-\pi/w_0)$	
II. $R\sin\psi<a$	
(a) $d_{\min}/c<\pi/w_0<d_{\max}/c$	
(i) $R\cos\psi<ct<d_{\min}$	$\ddot{u}_1$: $r_L(d)\mapsto r_u(d)$
(ii) $d_{\min}<ct<d_{\min}+\pi c/w_0$	$\ddot{u}_1$: $r_L(d)\mapsto a$
	$-\ddot{u}_1$: $r_L(d')\mapsto r_u(d')$
	$\ddot{u}_2$: $r_L(d')\mapsto r_u(d')$
(iii) $d_{\min}+\pi c/w_0<ct<d_{\max}$	$\ddot{u}_1$: $r_L(d)\mapsto r_u(d')$
	$\ddot{u}_2$: $r_u(d')\mapsto a$
(iv) $d_{\max}<ct<d_{\max}+\pi c/w_0$	$\ddot{u}_1$: $0\to a$
	$-\ddot{u}_1$: $r_L(d')\mapsto a$
	$\ddot{u}_2$: $r_L(d')\mapsto a$
(v) $d_{\max}+\pi c/w_0<ct$	$\ddot{u}_2$: $0\to a$
(b) $\pi/w_0<d_{\min}/c$	
(i) $R\cos\psi<ct<R\cos\psi+\pi c/w_0$	$\ddot{u}_1$: $r_L(d)\mapsto r_u(d)$
(ii) $R\cos\psi+\pi c/w_0<ct<d_{\min}$	$\ddot{u}_1$: $r_L(d)\mapsto r_u(d)$
	$-\ddot{u}_1$: $r_L(d')\mapsto r_u(d')$
	$\ddot{u}_2$: $r_L(d)\mapsto r_u(d)$
(iii) $d_{\min}<ct<d_{\min}+\pi c/w_0$	$\ddot{u}_1$: $r_u(d)\mapsto a$
	$-\ddot{u}_1$: $r_L(d')\mapsto r_u(d')$
(iv) Same as II.a.iii	
(v) Same as II.a.iv	
(vi) Same as II.a.v	
(c) $\pi/w_0>d_{\max}/c$	
(i) $R\cos\psi<ct<d_{\min}$	$\ddot{u}_1$: $r_L(d)\mapsto r_u(d)$
(ii) $d_{\min}<ct<d_{\max}$	$\ddot{u}_1$: $r_L(d)\mapsto a$
(iii) $d_{\max}<ct<\pi c/w_0$	$\ddot{u}_1$: $0\to a$
(iv) $\pi c/w_0<ct<\pi c/w_0+d_{\min}$	$\ddot{u}_1$: $0\to a$
	$-\ddot{u}_1$: $r_L(d')\mapsto r_u(d')$
	$\ddot{u}_2$: $r_L(d')\mapsto r_u(d')$
(v) $\pi c/w_0+d_{\min}<ct<\pi c/w_0+d_{\max}$	$\ddot{u}_1$: $0\to a$
	$-\ddot{u}_1$: $r_L(d')\mapsto a$
	$\ddot{u}_2$: $r_L(d')\mapsto a$
(vi) $\pi c/w_0+d_{\max}<ct$	$\ddot{u}_2$: $0\to a$
where $d=R\cos\psi+ct$ and $d'=R\cos\psi+c(t-\pi/w_0)$.	
III. $\psi=0$	
(a) $\pi/\omega_0<d_{\max}/c$	
(i) $R<ct<R+\pi c/w_0$	$\ddot{u}_1$: $0\to r_u(d)$
(ii) $R+\pi c/w_0<ct<d_{\max}$	$\ddot{u}_1$: $r_L(d')\mapsto r_u(d)$
	$\ddot{u}_2$: $0\to r_L(d')$
(iii) $d_{\max}<ct<d_{\max}+\pi c/w_0$	$\ddot{u}_1$: $r_u(d')\mapsto a$
	$\ddot{u}_2$: $0\to r_u(d')$
(iv) $d_{\max}+\pi c/w_0<ct$	$\ddot{u}_2$: $0\to a$
(b) $\pi/w_0>d_{\max}/c$	
(i) $r<ct<d_{\max}$	$\ddot{u}_1$: $0\to r_u(d)$
(ii) $d_{\max}<ct<\pi c/w_0$	$\ddot{u}_1$: $0\to a$
(iii) $\pi c/w_0<ct<\pi c/w_0+d_{\max}$	$\ddot{u}_1$: $r_u(d')\mapsto a$
	$\ddot{u}_2$: $0\to r_u(d')$
(iv) $\pi c/w_0+d_{\max}<ct$	$\ddot{u}_2$: $0\to a$
where $d_{\max}=(R^2+a^2)^{1/2}$, $d=R+ct$, $d'=R+c(t-\pi/w_0)$	

circles around the center of the plate. Integration is performed by dividing the plate into a number of annular rings and numerically integrating Eqs. (14) from the center of the plate up to each annular ring by using Simpson's rule. These values for I_i are then used in conjunction with the coefficients A_i and B_i in Eqs. (13) to obtain the sound pressure waveforms for different time periods given in Table I. The number of annular rings is chosen according to the frequency range of interest. In general, the higher this number is, the more accurate the results are.

An example of the sound pressure waveform from a centrally impacted circular plate obtained from Eq. (11) is given in Fig. 7 for the impact of a 1.905-cm-diam acrylic ball on a 1.59-mm-thick steel plate of 0.50-m diameter. The similarity between the sound pressure waveform and the corresponding velocity waveform at the center of the plate shown in Fig. 3 is noted for the initial pulse due to forced deformation of the plate.

III. EXPERIMENTS

Measurements corresponding to the present theoretical analysis were carried out to obtain plate vibration response and radiated acoustic pressure waveforms for different circular plates with clamped outer edge under various impact conditions. Steel and aluminum plates of 0.5-m diameter were clamped at the edges using sandwich circular rings bolted together. They were placed in a baffle with the radiating side facing an anechoic chamber, as shown in the schematic of the experimental apparatus in Fig. 8. The plates were impacted at their midpoints by an acrylic ball of 1.905-cm diameter and a steel ball of 1.27-cm diameter. The balls were dropped from various heights, H.

The acceleration and sound pressure waveform measurements were made using a subminiature accelerometer (B&K 8307) and a 1/8-in. D microphone (B&K 4138). Examples of measured sound pressure and plate acceleration waveforms corresponding to the calculated waveforms in Figs. 3 and 7 are given in Fig. 9.

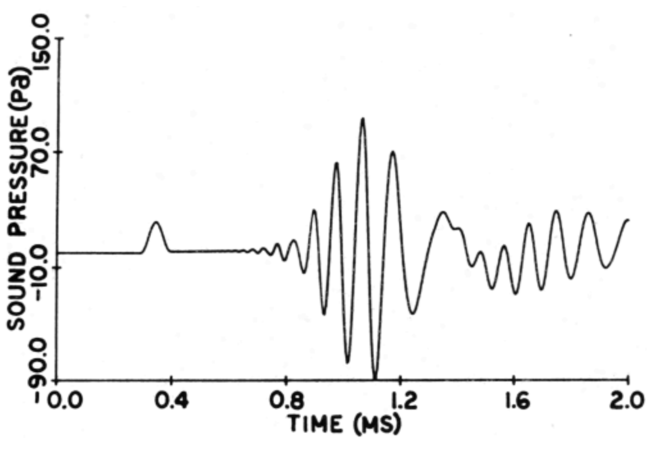

FIG. 7. Calculated sound pressure waveform on the axis of symmetry. $R = 0.10$ m, $H = 0.10$ m, $\eta = 0.05$.

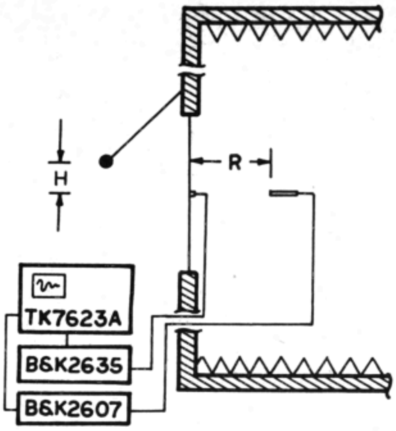

FIG. 8. Schematic of the experiment.

IV. RESULTS

The vibration and acoustic response of an impact-excited clamped circular plate has been obtained analytically. In the computations, contributions from the first 50 modes of the plate have been included. An equivalent value for the loss factor η has been selected from the experimental waveforms. One important assumption used in the analytical development was that the impacts were elastic or inelastic, with negligible plastic deformation. This assumption was very satisfactory for the impact of the acrylic ball on the plates. For the impact of the steel ball on the plates considered here, the analytical results differ from the experimental results. This difference increased at higher impact velocities.

The velocity response of the plate at the impact point shows the same waveform as that of the impact force during contact. This follows from the real and frequency independent impedance of the plate. The contact force waveform,

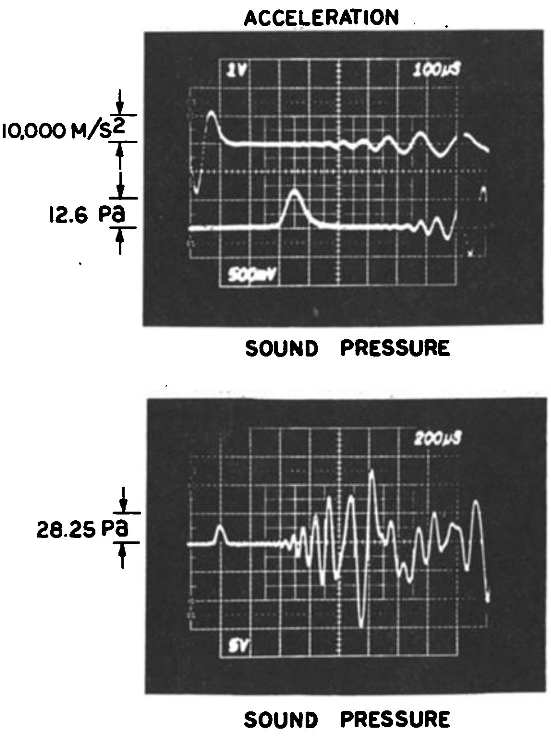

FIG. 9. Measured sound pressure and plate acceleration waveforms.

calculated from the response of a plate to the Hertz impact force, was calculated as a function of an inelasticity parameter λ and plotted in Figs. 1 and 2. The effect of inelasticity can be considered as spreading the collision energy over a longer period of time, thus reducing the impact force magnitude. For $\lambda = 0$ the forced response corresponds to the contact force calculated from Hertz theory, as in the case of the elastic impact of a ball on a very thick plate or slab. These results were obtained for large plates. For small plates where the reflection of bending waves returns to the impact area during the contact period, the effect of the resonance of the plate must also be included in these calculations.[21]

The effects of the choice of the impact-force time history are illustrated in Fig. 10 for the 1, 1.5, and 2nd powers of a half-period sine wave. It is seen that the half-period sine wave induced discontinuities in the acceleration response of the plate during contact, whereas the 1.5 and 2nd powers of the same force history are similar to each other and to the experimental results, with a smooth beginning and end.

The theoretical and measured peak acceleration responses of the plates on the other side of the impact point are tabulated in Table II. These results show good agreement between analytical and experimental values and demonstrate the effects of departure from the assumptions of elastic impact and from Hertz theory.

The peak sound pressure values computed from the analytical results agree well with the measured values for the more elastic impacts, as shown in Table III. As in the case of the vibration response, the agreement is less for the impact of the steel ball on the plates.

TABLE II. Calculated and measured values of peak acceleration values of plates during impact. Plates are 1.59-mm thick with 0.5-m diameter.

1.905-cm-diam acrylic ball

	(m/s²)			
	Aluminum plate		Steel plate	
U_0(m/s)	Calculated	Measured	Calculated	Measured
0.44	6 250	6 000	3 700	3 600
0.62	9 890	9 500	5 830	6 000
0.88	15 650	16 000	9 330	9 500
1.40	27 830	28 000	17 110	17 000

1.27-cm-diam steel ball

	(m/s²)			
	Aluminum plate		Steel plate	
U_0(m/s)	Calculated	Measured	Calculated	Measured
0.44	16 930	19 000	18 900	18 500
0.62	26 320	34 000	28 870	29 000
0.88	40 730	47 500	44 340	50 000
1.40	71 150	95 000	81 030	105 000

V. DISCUSSION

The similarity between the force-, velocity-, and pressure-time histories for the initial pulse is apparent both in the analytical and experimental results. The initial pulse in the plate velocity and sound pressure waveform is due to the forced deformation of the plate. Both the theoretical and experimental results show that, immediately following the initial sound pressure pulse, there is no sound radiation until the bending waves are reflected back from the edge to the center of the plate, reaching a state of damped free vibrations. The lack of contribution of the bending waves before resonant vibrations are started can be explained by considering the radiation mechanism from the bending waves of the plates. Below the critical frequency, bending waves do not radiate any acoustic power. On the other hand, at and above the critical frequency the direction of radiation is away from the axis of symmetry and is determined by the ratio of the wavelengths of the plate bending waves and sound pressure. This can be verified by measuring sound pressure off the axis of symmetry, as shown in Fig. 11. As the measurement point is moved away from the axis of symmetry, radiation from the bending waves starts to reach the receiver point before the "pulse" and there is no "silent" time period before the resonance takes place as was the case for $\psi = 0$. This phenomenon has also been observed in larger plates of arbitrary

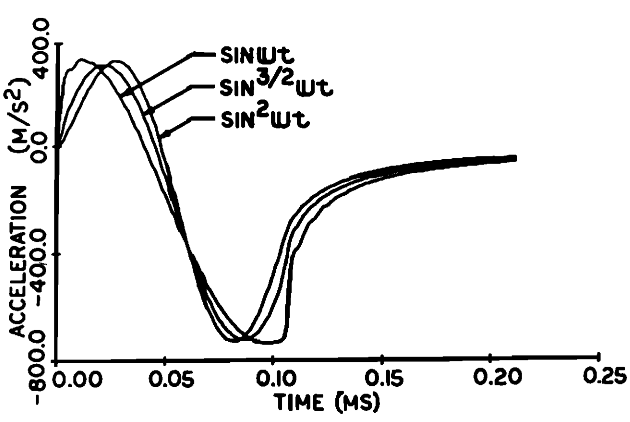

FIG. 10. Vibration response to different force-time histories.

TABLE III. Calculated and measured values of peak sound pressure levels of the "initial pulse" for various impact conditions.

	(dB)		(dB)	
	Calculated	Measured	Calculated	Measured
U_0(m/s)	$R = 0.10$ m, $\psi = 0°$		$R = 0.50$ m, $\psi = 0°$	
Impact of 1.905-cm-diam acrylic ball and 0.5-m-diam aluminum plate				
0.44	115	114	103	100.5
0.62	118	117	105	104
0.88	122	120	110	108
1.40	126	125	113	112
Impact of 1.905-cm-diam acrylic ball and 0.5-m-diam steel plate				
0.44	110	107	97	95.5
0.62	113.5	111	102	98
0.88	117	115.5	105	102.5
1.40	121	118	108	106

shape.[25] It can be concluded that the initial pulse is due to the rapid deformation of the impacted region of the plate, which acts like a piston with a spatially and temporally varying velocity profile. An illustration of this can be seen in Fig. 12 where a smaller sound pressure pulse precedes the usual radiation. This smaller sound pressure waveform is due to the flat end of the accelerometer placed on the plate on the opposite side from the impact point. The time delay between the pulses is accounted for by the early arrival of the waves from the accelerometer surface which is closer to the receiver point. It should be noted, however, that the plate deformation during contact does not generate sound as a rigid piston where contribution from the edge diffraction contributes to the sound field.

The radiation mechanism during resonance is similar to steady-state radiation from circular plates and has been treated in the literature. In this case, the plate vibrations can be considered as an array of concentric circles with different amplitude and phase relationships as was done in the numerical integrations here. This array of sources lead to enhancement and cancellation of sound at different frequencies due to the phase differences introduced by the vibration response and the distance of the receiver to different elements on the plate.

A brief examination of Eq. (12) reveals the important parameters in impact sound generation. It is clear that sound pressure is directly proportional to the impact force and inversely proportional to the mass of the plate. Although not explicitly apparent in the equation, mechanical impedance of the plate has dual and opposite roles. The lower the impedance of the plate the higher the "inelasticity parameter" becomes thereby reducing the impact force amplitude during contact. On the other hand, lower impedance values result in higher drive point velocity of the plate. From Fig. 2, the dependence of the impact force on the inelasticity parameter can be approximated as

$$F_0 = F_H(1 - e^{-\lambda}). \tag{15}$$

From this relationship, the impact velocity v can be obtained as

$$v = F_H\,[1 - \exp(-3.321\, m/T_H Z)]/Z. \tag{16}$$

Equation (16) has been plotted for various impact conditions in Fig. 13 to illustrate the dual role of the plate impedance on the drive point response of the plate. It is clear that above a certain value further increase in impedance does not effectively reduce the plate mobility.

The empirical relationship offered by previous studies[4–8] relating sound pressure and acceleration levels of impacted plates to the kinetic energy of the striker can be readily obtained from Eq. (12). Substitution for the impact force amplitude F_0 from Eqs. (5) and (15) and regrouping of the terms result in an expression as

$$\mathrm{SPL} = 12 \log E + 20 \log[C_1 C_2] + 81\ \mathrm{dB}, \tag{17}$$

where $C_1 = k^{0.4}(1 - e^{-\lambda})/M$ and C_2 is the expression inside the summation sign in Eq. (12). It is clear here that the

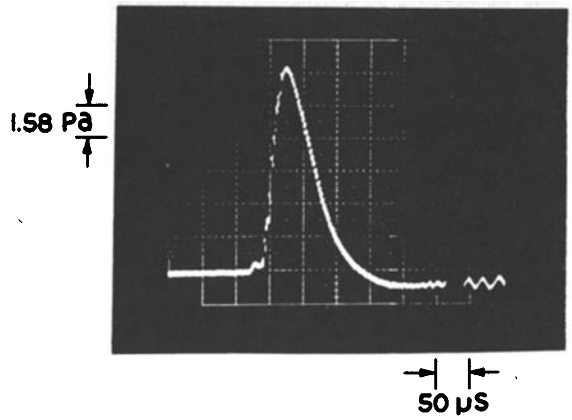

FIG. 12. Sound pressure waveform at $R = 0.10$ m.

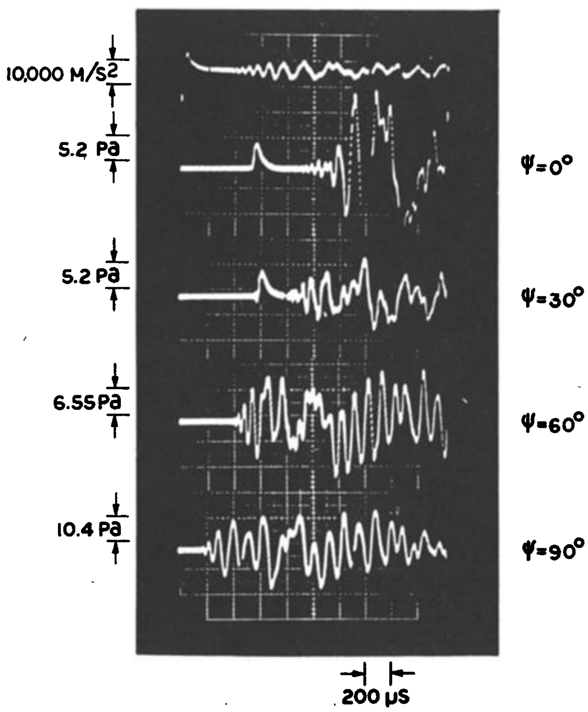

FIG. 11. Sound pressure waveforms away from the axis of symmetry.

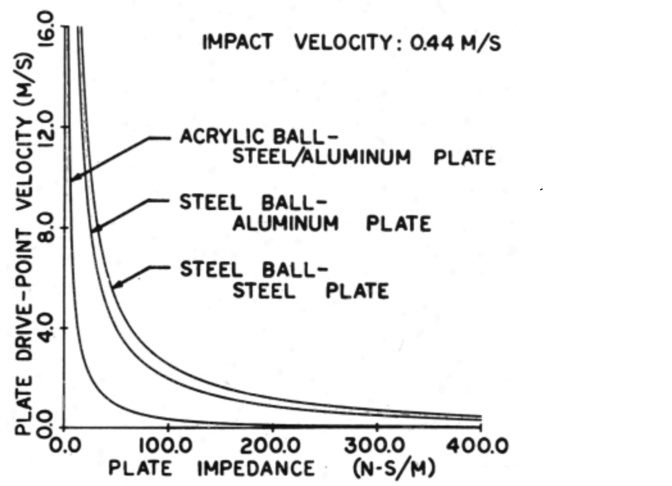

FIG. 13. Drive point velocity response of a plate to impact forces as a function of plate impedance.

value C_1 which represents the plate response and radiation characteristics, is a determining factor of the SPL and extensive numerical simulations can give some generalized results. However, the slope of the equation between SPL and the kinetic energy of the striker is always constant and is verified by earlier results.[8]

VI. CONCLUSIONS

Axisymmetric sound radiation from an impact excited clamped plate has been obtained. Since the approximations were kept to a minimum, the results are applicable to both near- and farfields. The numerical scheme used reduces the computation time even for very high spatial and frequency resolutions.

The experimental and analytical results show a sound pulse emanating from the impact region of the plate. It is also observed that the outgoing bending waves do not contribute to the acoustic pressure on the axis of impact leading to the conclusion that for very large and heavily damped plates the initial sound pressure pulse may be the dominant source of sound on the axis of impact.

Although the results for axisymmetric excitation and radiation are given here, the present method can be extended to asymmetric problems.

ACKNOWLEDGMENTS

The authors gratefully acknowledge partial support for this research from the Wayne State University Development Fund and the National Science Foundation.

[1] A. Akay, "A review of impact noise," J. Acoust. Soc. Am. **64**, 977–987 (1978).

[2] M. Strasberg, "Radiation from a diaphragm struck periodically by a light mass," J. Acoust. Soc. Am. **20**, 683–690 (1948).

[3] M. Lax, "The effect of radiation on the vibrations of a circular diaphragm," J. Acoust. Soc. Am. **16**, 5–13 (1944).

[4] Y. Tokita, "Vibration of a plate and sound radiation generated by an impulse force," J. Phys. Soc. Jpn. **16**, 1008–1019 (1961).

[5] Y. Tokita, "Vibration and sound radiation of a plate generated by an impulse force (I)," J. Acoust. Soc. Jpn. **16**(3), 170–177 (1960).

[6] Y. Tokita, "Vibration and sound radiation of a plate generated by an impulse force (II)," J. Acoust. Soc. Jpn. **17**(2), 116–122 (1961).

[7] J. L. Beiers, "A study of noise sources in pneumatic rock drills," J. Sound Vib. **3**, 166–194 (1966).

[8] A. Akay, T. H. Hodgson, and J. R. Bailey, "Sound radiation from the impact of a sphere on an elastic plate," ASME Paper No. 75-DET-51 (1975).

[9] E. B. Magrab and W. T. Reader, "Farfield radiation from an infinite elastic plate excited by a transient point loading," J. Acoust. Soc. Am. **44**, 1623–1627 (1968).

[10] A. D. Stuart, "Acoustic radiation from a point excited infinite elastic plate," Ph.D. dissertation, The Pennsylvania State University, 1972.

[11] S. S. Mackertich and S. I. Hayek, "Acoustic radiation from an impulsively excited elastic plate," J. Acoust. Soc. Am. **69**, 1021–1028 (1981).

[12] I. Nakayama, A. Nakamura, and R. Takeuchi, "Insulation characteristics of a circular plate for a single sound pulse," Jpn. J. Appl. Phys. **16**, 2285 (1977).

[13] I. Nakayama, A. Nakamura, and R. Takeuchi, "Transmission characteristics of sound pulse through a circular plate," Acustica **40**, 40 (1978).

[14] I. Nakayama, A. Nakamura, and R. Takeuchi, "Transient radiation field from an elastic circular plate excited by a sound pulse," Acustica **46**, 276–282 (1980).

[15] I. Nakayama, "Sound insulation of a circular plate for a single sound pulse," Acustica **46**, 330–340 (1980).

[16] I. Nakayama and A. Nakamura, "Mechanism of transient sound radiation from a circular plate for impulsive sound wave," J. Acoust. Soc. Jpn. (E)**2**, 151–159 (1981).

[17] I. J. Busch-Vishniac and R. H. Lyon, "Paper noise in an impact line printer," J. Acoust. Soc. Am. **70**, 1679–1689 (1982).

[18] S. C. Hunter, "Energy absorbed by elastic waves during impact," J. Mech. Phys. Solids **5**, 162–171 (1957).

[19] A. E. H. Love, *A Treatise on the Mathematical Theory of Elasticity* (Dover, New York, 1944), 4th ed., 198–200.

[20] W. Goldsmith, *Impact* (Edward Arnold, London, 1960), pp. 82–144.

[21] K. Karas, "Platten unter seitlichem Stoss," Ingenieur Archiv. **10**, 237–250 (1939).

[22] C. Zener, "Intrinsic inelasticity of large plates," Phys. Rev. **59**, 669–673 (1941).

[23] W. Goldsmith, T. W. Lin, and S. Chulay, "Plate impact and perforation by projectiles," Exp. Mech. **5**, 385–404 (1965).

[24] Lord Rayleigh, *Theory of Sound*, Vol. II (Dover, New York, 1945), Sec. 278.

[25] A. Akay and R. O. Cook, "Sound radiation due to rapid deformation of an impacted plate," J. Acoust. Soc. Am. Suppl. 1 **64**, S174 (1978).